The mammalian SKI complex is a broad-spectrum antiviral drug target that upregulates cellular cholesterol to inhibit viral replication

Short Title: Drug targeting the SKI complex increases cellular cholesterol

Stuart Weston[a], Lauren Baracco[a], Louis Taylor[a], Alison Scott[b,c], Gaurav Kumar[d], Paul Shapiro[d], Alexander D. MacKerell Jr. [d], and Matthew B. Frieman[a*]

[a] Center for Pathogen Research, Department of Microbiology and Immunology, University of Maryland School of Medicine, Baltimore, MD, 21201

[b] Department of Microbial Pathogenesis, University of Maryland School of Dentistry, Baltimore, MD, 21201

[c] Department of Microbiology and Immunology, University of Maryland School of Dentistry, Baltimore, MD, 21201

[d] Department of Pharmaceutical Sciences, University of Maryland School of Pharmacy, Baltimore, MD, 20201

* Corresponding author: MFrieman@som.umaryland.edu

Abstract

There is a need for the development of broad-spectrum antiviral compounds that can act as first line therapeutic countermeasures to emerging viral infections. Host-directed approaches present a promising avenue of development and carry the benefit of mitigating risks of viral escape mutants. We have previously found the SKI (super killer) complex to be a broad-spectrum, host-target with our lead compound ("UMB18") showing activity against influenza, coronaviruses, and filoviruses. The SKI complex is a cytosolic RNA helicase and we previously found that targeting it with UMB18 inhibited viral RNA production but did not further define the mechanism. Here, transcriptomic analysis of UMB18 treated A549 cells revealed an upregulation of genes in the mevalonate pathway which drives cholesterol synthesis. Further investigation validated the genetic upregulation and confirmed an increase in total cellular cholesterol. This upregulation was dependent on the SKI complex, the sterol regulatory element binding proteins (SREBPs) and their regulator SCAP, the major regulators for cholesterol and fatty acid synthesis. Depletion of the SREBPs or SCAP with siRNA, or extraction of cholesterol with methyl β-cyclodextrin attenuated UMB18 antiviral activity, emphasizing the role of increased cholesterol synthesis in this mechanism of action. Our findings further define the antiviral mechanism of a developmental host-directed therapeutic approach with broad applicability against emerging viral pathogens.

Author Summary

The COVID-19 pandemic has underscored the urgent need for effective countermeasures to novel and emerging viral pathogens. Our research presented here builds upon our previously published data on an experimental novel antiviral compound termed UMB18. We have found this compound capable of inhibiting replication of influenza A virus, coronaviruses and the filoviruses Marburg and Ebola virus, but did not fully define a mechanism of action. In this work, we demonstrate that UMB18 exerts antiviral activity by modulating cellular cholesterol levels. By targeting the SKI complex, UMB18 triggers an increase in endogenous cellular cholesterol which disrupts the fine balance viruses rely on for efficient infection. We demonstrate that this mechanism inhibits replication of SARS-CoV-2, revealing a previously undescribed host-directed strategy for antiviral intervention. These findings highlight UMB18's potential as a broad-spectrum antiviral agent and pave the way for further research into its mechanism and therapeutic applications, offering a promising avenue for development of antiviral countermeasures to current, novel and emerging pathogens.

Introduction

The COVID-19 pandemic has highlighted the lack of broadly acting therapeutics to treat coronaviruses as well as other emerging pathogens. When severe acute respiratory syndrome coronavirus-2 (SARS-CoV-2) emerged and spread globally there were few countermeasures available for treating coronavirus disease-2019 (COVID-19) resulting in a reliance on non-pharmacological interventions of physical distancing and isolation to control the outbreak. While those measures helped to some degree, the continued pandemic spread of the virus highlighted the urgent need for novel therapeutics against emerging viral disease. Fortunately, vaccines were developed at a record pace and contributed significantly to the management of COVID-19. However, the ongoing threat of emerging viral pathogens necessitates the development of complementary strategies. Broad-spectrum antiviral chemical compounds could serve as rapid, first-line countermeasures against emerging pathogens, filling a crucial gap before specific measures can be developed. Addressing this need, our research is focused on a host-directed approach of targeting the SKI (super killer) complex(1).

While using host-directed therapeutics may come at a cost of having certain side effects, there is a significantly lower risk of viral escape mutants developing owing to the varying mutation rate of host versus virus. The risk of virus evolution to escape countermeasures is perfectly demonstrated by the dwindling number of effective monoclonal antibodies available to treat COVID-19 patients through mutation of the spike protein in SARS-CoV-2 variants(2). Direct acting nucleoside analogues have been implicated in increasing the risk of viral mutagenesis posing concerns for vaccine and

80 monoclonal antibody treatments(3). Targeting host factors that do not directly affect the
81 viral genome could alleviates these concerns.
82
83 We focus on the SKI complex, a eukaryotic protein complex we previously identified
84 through a yeast-based screening system to be a proviral factor(1). Comprising SKIC2,
85 SKIC3, and SKIC8 (formerly SKIV2L, TTC37, and WDR61, respectively) the SKI
86 complex acts as a cofactor to the cytosolic RNA exosome to facilitate 3' to 5' RNA
87 degradation(4–6). SKIC2 is a member of the DExD/H helicase family, while SKIC3 and
88 SKIC8 have structural and regulatory functions(7). The complex was first defined in
89 yeast where it was implicated in resistance to the "super killer" toxin of a yeast double
90 stranded RNA virus, hence the naming convention of SKI(8,9). Our previous study
91 demonstrated that siRNA depletion of the SKI complex inhibited replication of influenza
92 A virus (IAV) and Middle East respiratory syndrome coronavirus (MERS-CoV). We
93 proceeded to investigate chemical compounds that were *in silico* predicted to bind to
94 SKIC8 and potentially disrupt the proviral activity of the SKI complex. This work
95 generated multiple chemical scaffold structures that inhibited both IAV and MERS-CoV,
96 in agreement with our siRNA studies, but additionally inhibited SARS-CoV, SARS-CoV-
97 2, and the filoviruses Ebola and Marburg. We demonstrated that our lead compound,
98 termed UMB18, did not significantly inhibit IAV entry to cells, but potently inhibited RNA
99 and subsequent protein production in single-cycle infections and therefore imposed
100 antiviral activity. Our previous work defined UMB18 as a host-directed antiviral, targeting
101 post-entry steps prior to RNA production, with broad-spectrum activity(1).
102

103 This study aimed to elucidate the mechanism of the antiviral activity of UMB18. Using
104 RNA sequencing of cells treated with UMB18, with and without SARS-CoV-2 infection,
105 we identified a significant upregulation of genes in the mevalonate pathway, which is
106 crucial for cholesterol synthesis, regardless of viral infection status. Cholesterol is an
107 essential lipid found throughout cellular membranes which at high levels causes an
108 increased rigidity, it is also a major part of hormone and oxysterol production.
109 Cholesterol can be obtained from external sources through low-density lipoprotein (LDL)
110 receptors or endogenously synthesized through the mevalonate pathway(10–12). This
111 cholesterol synthesis pathway has many other useful metabolic products for the cell and
112 is involved with protein prenylation, such that there must be tight regulation between
113 uptake from external sources and endogenous synthesis of cholesterol. Activation of
114 this pathway by UMB18 suggests a previously unknown antiviral mechanism of action
115 for our developmental compound.
116
117 Sterol regulatory element binding proteins (SREBPs) are master regulators of
118 cholesterol and fatty acid synthesis through upregulating genes involved in both
119 synthesis pathways(13). SREBPs comprise three isoforms, SREBP1a, SREBP1c, and
120 SREBP2, expressed from two genes *Srebf1* and *Srebf2*(14). Each isoform has an
121 equivalent tripartite structure with an N-terminal basic-helix-loop-helix leucine zipper
122 family transcriptional domain, a short hairpin transmembrane domain, and a C-terminal
123 domain involved in protein-protein interactions(13,14). SREBP1a and SREBP1c are
124 produced from alternate transcriptional start sites which alters their N-terminal domains
125 and their sterol regulator element (SRE) binding specificity(15). SREBP2 is roughly 50%

126 identical to SREBP1 at the amino acid level. It is generally considered that SREBP1c is
127 mostly involved in expression of lipogenic genes, SREPB1a can regulate both lipid and
128 cholesterol synthesis genes, while SREBP2 is mostly involved in cholesterol
129 synthesis(16,17).
130
131 *Srebf* genes produce inactive precursor proteins that localize to the endoplasmic
132 reticulum (ER) where they associate to SREBP cleavage-activating protein (SCAP).
133 Cholesterol binding to SCAP causes a conformation that results in retention of the
134 SCAP-SREBP complex at the ER. However, low cholesterol levels cause a
135 conformational change to SCAP, exposing a MELADL motif that directs COPII-coated
136 vesicle trafficking of the SCAP-SREBP complex to the Golgi apparatus(18,19). At the
137 Golgi, SREBP proteins are cleaved by signal peptidase 1 and 2 to free the N-terminal
138 transcription factor domain for nuclear translocation(13,20). Cleavage-activated SREBP
139 binds SREs and initiates transcription of genes in both fatty acid and cholesterol
140 synthesis pathways.
141
142 In the present study, transcriptomic analysis revealed that our SKI-targeting compound
143 UMB18 caused an upregulation of genes involved in cholesterol synthesis, a finding we
144 confirmed with qRT-PCR. In agreement with the RNA-based increase in cholesterol
145 synthesis genes we also saw an increase in total cellular cholesterol using mass
146 spectrometry. UMB18 was found to bind SKIC8 through *in vitro* expression and binding
147 assays and the transcriptional changes were dependent on the presence of SKI
148 complex since these were reduced by siRNA-mediated depletion of SKI genes, where

149 SKIC8 depletion had the greatest effect. Further, depletion of *Srebf1* or *Srebf2* reduced
150 UMB18-mediated increases in mevalonate pathway genes, indicating that UMB18 acts
151 through the canonical pathway for endogenous cholesterol synthesis. Notably, UMB18
152 antiviral activity against SARS-CoV-2 was significantly reduced with either depletion of
153 the *Scap* or *Srebf* genes or extraction of cholesterol with methyl-β cyclodextrin. These
154 results underscore the importance of increased total cellular cholesterol in the
155 mechanism of action for UMB18 as an antiviral compound.
156
157 Overall, the work presented here builds upon our previous study demonstrating the
158 promise of UMB18 as a broad-spectrum, host-directed antiviral compound and
159 elucidates its mechanism of action through upregulation of cellular cholesterol synthesis
160 by targeting the SKI complex.
161

162 Results

163 **Transcriptomic profiles show UMB18 upregulates genes involved in cholesterol**
164 **synthesis.**
165 Having previously described the broad-spectrum antiviral activity of the SKI-targeting
166 compound UMB18(1), we aimed to better identify the mechanism of action for the
167 compound. To this end we utilized RNA transcriptomic analysis of treated and/or SARS-
168 CoV-2 infected cells *in vitro*. A549 cells (human lung alveolar adenocarcinoma cells)
169 overexpressing human angiotensin converting enzyme 2 (A549-ACE2) to allow for
170 SARS-CoV-2 infection were used for the transcriptomic analysis and four conditions
171 were analyzed: 10μM UMB18 treatment, 0.1% DMSO treatment (carrier for UMB18),

172 10μM UMB18 with SARS-CoV-2 infection or 0.1% DMSO with SARS-CoV-2 infection.
173 We previously found 10μM to be inhibitory to viral replication with no cytotoxicity(1). All
174 infections were at multiplicity of infection (MOI) 0.1 and across two experiments with
175 either 24-hour (h) and 48 h or just a 24 h time point were analyzed. In uninfected cells,
176 UMB18 treatment resulted in increased expression of mevalonate pathway genes at 24
177 h and 48 h compared to uninfected, DMSO-treated cells (Fig. 1A). Pathway analysis
178 revealed an enrichment in pathways associated with cholesterol biosynthesis, which
179 were predicted to have increased activity based on the patterns of differential
180 expression of genes within the pathway (Fig. 1B). Mevalonate pathway genes are
181 upregulated with UMB18 treatment at both 24 h and 48 h relative to DMSO-treated
182 controls, regardless of infection with SARS-CoV-2 (Fig. 1C). SARS-CoV-2 infection had
183 minimal impact on the mevalonate pathway, probably because we used bulk RNA
184 sequencing and 10μM UMB18 caused a roughly 90% inhibition of infection meaning
185 only low levels of SARS-CoV-2 replication are occurring in the treated cells (for example
186 see Fig. 5F). This analysis demonstrated upregulation of genes involved in the
187 mevalonate pathway after treatment with UMB18, potentially linking the SKI complex
188 with cholesterol synthesis.
189
190 **Increase in cholesterol levels in UMB18 treated cells.**
191 The upregulation of the mevalonate pathway through the transcriptomic analysis
192 suggested that cholesterol synthesis may be affected by UMB18. We validated the
193 results of the transcriptomic analysis using qRT-PCR with primers targeting a subset of
194 the genes in the mevalonate pathway. Identical to the previous experiment, A549-ACE2

195 cells were treated with 10μM UMB18 or 0.1% DMSO as the vehicle control for 24 or
196 48h. Additionally, A549 cells not expressing ACE2 were subject to the same treatments
197 to further validate the results and ensure that ACE2 overexpression is not impacting the
198 transcriptional changes. Seven genes for enzymes involved in various stages of the
199 mevalonate pathway were analyzed to get a broad view of transcriptional changes
200 (pathway schematic in Fig. 2A, yellow boxes are selected genes for analysis). Relative
201 to DMSO treatment, UMB18 caused an increase in expression of genes in the
202 mevalonate pathway, ranging from approximately 2- to 6-fold. In the A549-ACE2 cells
203 (Fig. 2B), the induction of the selected genes peaked at 24h and then declined by 48h,
204 yet remain above the levels observed in DMSO-treated cells, while in the A549 cells
205 (Fig. 2C) there was an increase or at least stability of the change observed across the
206 full 48 h. Even though there was a minor difference in the temporal dynamics, the
207 magnitude of change was largely equivalent between the two cell lines, and we suspect
208 these differences are artifacts of using cell culture systems with the base A549 cells
209 having two different backgrounds (see Materials and Methods), rather than an impact of
210 ACE2 expression. Overall, these qRT-PCR data suggest that UMB18 caused an
211 increase in genes that regulate cholesterol synthesis through the mevalonate pathway
212 and that the expression of ACE2, which allows for infection by SARS-CoV-2 (which will
213 be used later in this study), does not significantly alter the magnitude of change.
214
215 These experiments were performed in serum supplemented media and therefore have
216 exogenous cholesterol available. Cells can endocytose cholesterol through the LDL-
217 receptor and activate a negative feedback loop to inhibit the mevalonate pathway. It

218 therefore appears UMB18 may activate this metabolic pathway even in the presence of
219 exogenous cholesterol. To further analyze the system, we treated A549-ACE2 cells with
220 UMB18 or DMSO in serum-containing or serum-free media, harvested at 24 hours, and
221 performed qRT-PCR for a subset of the mevalonate pathway genes. In serum-
222 containing media, UMB18 treatment resulted in a similar increased gene expression.
223 However, no significant differences were noted in serum-free media (Fig. S1A). In the
224 absence of exogenous cholesterol, cells likely activate the mevalonate pathway to
225 promote endogenous synthesis. Analysis of DMSO treated cells demonstrated a 6-7-
226 fold increase in expression of three mevalonate pathway genes in serum-free compared
227 to serum-containing media (Fig. S1B). We hypothesize that the lack of UMB18 effect in
228 serum-free media (Fig. S1A) is due to the pathway already being activated in response
229 to cholesterol-deprivation resulting in UMB18 having minimal additional impact on this
230 pathway. Supporting this hypothesis, UMB18 treatment in serum-free media showed
231 only a 2-fold increase in gene expression compared to serum-containing media, in
232 contrast to the 6-7-fold increase with DMSO (Fig. S1B). Consequently, since UMB18
233 and serum depravation both increase mevalonate pathway gene expression, their
234 combination results in minimal additive effects on the mevalonate pathway gene
235 expression. These results, which have implications for viral replication (Fig. S1C) to be
236 discussed later, demonstrate that UMB18 treatment induces expression of mevalonate
237 pathway genes in a manner comparable to the absence of serum.
238
239 With there being an increase in the expression of genes involved in the mevalonate
240 pathway, we next investigated whether total cellular cholesterol was increased in the

241 cells. To this end, we utilized silver-assisted laser desorption ionization mass
242 spectrometry imaging (Ag-LDI MSI), a highly sensitive method of detecting total cellular
243 cholesterol, of A549-ACE2 cells treated with UMB18 or DMSO. Cell culture monolayers
244 treated with UMB18 showed a higher intensity of cholesterol signal compared to DMSO-
245 treated cells. Cholesterol was detected and visualized in the monolayers as the ion *m/z*
246 493.260 +/- 2.2 mDa ([cholesterol+Ag_{107}]$^{+}$) ion (Fig. 2D) and the silver isotopologue ion
247 [cholesterol+Ag_{109}]$^{+}$ data were in agreement. Treatment with UMB18 resulted in a
248 significant increase in relative cholesterol abundance, showing a nearly 2-fold increase
249 in pixel intensities. Further, a receiver-operator characteristic analysis showed an area-
250 under-the-curve value of 0.804 for cholesterol in UMB18 treated cells, making
251 cholesterol abundance a strong discriminator over DMSO-treated cells. These data
252 demonstrate that UMB18 treatment of A549-ACE2 cells results in significantly and
253 discriminatorily higher amounts of cholesterol compared to control.
254
255 **UMB18 directly binds SKIC8 and the SKI complex is required for increasing**
256 **mevalonate pathway genes.**
257 Since UMB18 treatment caused an increase in cellular cholesterol through
258 transcriptional regulation of genes involved in the mevalonate pathway, we wanted to
259 ensure that this response was through specificity of UMB18 targeting the SKI complex.
260 We previously developed the compound using an *in silico* modeling approach, with the
261 compound predicted to bind to SKIC8 (formerly WDR61), and showed that the genes of
262 the SKI complex were required in cells for the antiviral activity, thus suggesting

263 specificity(1). However, whether the increase in cholesterol is a consequence of
264 targeting the SKI complex needs to be established.
265
266 In our previous work, UMB18 was modeled to target SKIC8 at the binding interface with
267 SKIC3 (formerly TTC37). We wanted to establish that the predicted binding is seen *in*
268 *vitro* and to that end, expressed and purified SKIC8 from bacterial cells and analyzed
269 UMB18 binding by surface plasmon resonance (SPR). The fast association and
270 dissociation rate constants observed at various compound concentrations indicated
271 binding to the SKIC8 target with a relatively low binding affinity, K_D = 81 μM (Fig. 3A).
272
273 We next tested whether the SKI complex was important for the observed increase in
274 mevalonate pathway genes. A549-ACE2 cells were transfected with siRNA sequences
275 targeting each of the three SKI genes, SKIC2 (formerly SKIV2L), SKIC3, and SKIC8, for
276 individual knockdown and then treated with UMB18 or DMSO before analysis of
277 mevalonate pathway genes by qRT-PCR. Cells were siRNA transfected for 72 h and
278 treated with UMB18 or DMSO for 24 h before collection for qRT-PCR with three select
279 target genes (MVD, FPDS and MSMO1), which target different parts of the pathway as
280 displayed in Fig. 2A. The SKI siRNA knockdowns were stable throughout the 96 h of
281 experiment time and were gene-specific (Fig. 3B). Moreover, UMB18 treatment of cells
282 did not impact the knockdown nor expression of the SKI genes as compared to DMSO
283 (Fig. 3B), with no significant different seen between UMB18 and DMSO treated siRNA
284 transfected cells. In each of the paired UMB18 or DMSO knockdowns, a relative level of
285 expression of 33 and 35% was achieved for SKIC2 (UMB18 and DMSO respectively),

286 20 and 20% for SKIC3 and 21% and 20% for SKIC8, all relative to scrambled siRNA
287 with DMSO.
288
289 Transfection of scrambled siRNA did not alter the ability of UMB18 to increase the level
290 of transcript for the mevalonate pathway genes. There were statistically significant
291 differences in the ΔCt values between UMB18 and DMSO treated conditions for all
292 three genes (Fig. 3C-E). For analyzing the effect of SKI siRNA transfection on changes
293 in mevalonate genes, the ΔΔCT was calculated and plotted as relative fold change to
294 scrambled siRNA (Scr) transfected cells treated with DMSO treatment (Scr/DMSO) as
295 the control for all conditions (Fig. 3C). There was still an increase in the mevalonate
296 genes in the SKI siRNA cells compare to DMSO. However, the only statistically
297 significant differences were seen for MVD and MSMO1 in the context of SKIC3 siRNA.
298 No statistically significant differences were seen in any of the SKIC2 or SKIC8 pairwise
299 comparisons by two-way ANOVA analysis. This lack of statiscally significant difference
300 suggests that the loss of the SKI complex removes the change caused by UMB18
301 treatment, even though there is still an increase in expression. To better analyze these
302 changes, the fold change relative to Scr/DMSO of Fig. 3C can be set as fold change of
303 UMB18 in SKI siRNA compared to scrambled siRNA to assess the impact that
304 knockdown of SKI genes has. In this analysis, if the relative fold change is 1, there
305 would be no change from the knockdown of SKI gene expression, were it to be greater
306 than 1, the loss of the SKI genes would be enhancing the effect, and were it be below 1,
307 this suggests that loss of the SKI genes is attenuating the UMB18-mediated increase in
308 mevalonate pathway genes. Knockdown of the enzymatic SKIC2 had little impact on the

309 increase of the mevalonate genes, yet there is a reduction in the UMB18-induced
310 increase when SKIC3 and SKIC8 are reduced. SKIC8 had the most pronounced effect,
311 causing roughly a 40% decline in the increase in mevalonate gene expression. Since
312 UMB18 targets SKIC8 at the interface of SKIC3 and SKCI8 we interpret these data as
313 evidence that the SKI complex is indeed involved in UMB18's induction of the
314 mevalonate pathway.
315
316 **SCAP and SREBP are required for UMB18-induced increases in mevalonate**
317 **pathway genes.**
318 Our data suggest that UMB18 binds to the SKI complex and consequently increases
319 expression of genes in the mevalonate pathway leading to an increase in total cellular
320 cholesterol. We set out to determine what cellular pathways the SKI complex might be
321 interacting with to mediate this effect. First, we looked at the mammalian target of
322 rapamycin (mTOR) complex because of recently published findings that demonstrated
323 that a loss of SKIC2 activity was connected to an increase in mTORC1 signaling(21).
324 The mTOR complex is a master regulator of numerous aspects of cellular metabolism
325 and of interest to our research it can regulate activation of the sterol regulatory element
326 binding proteins (SREBPs) which promote expression of the mevalonate genes. We
327 analyzed the ribosomal protein S6 kinase 1 (S6K1) which is phosphorylated of when the
328 mTOR pathway is activated. Using treatment with epidermal growth factor (EGF), a
329 known activator of the mTOR pathway, we were able to detect phospho-S6K1 (pS6K1),
330 demonstrating that our cells show a canonical marker for mTOR signaling (Fig. S2B).
331 We proceeded to treat cells with UMB18 for various time points, either longer times that

332 match our other treatments (Fig. S2B) or shorter times (Fig. S2C). However, none of
333 these experiments showed any significant changes to phospho-S6K1, suggesting that
334 UMB18 wasn't causing a detectable activation of mTOR, at least based on
335 phosphorylation of S6K1.
336
337 While UMB18 did not showing any clear activation of mTOR, we next investigated the
338 downstream target that was more directly relevant to our data of increased mevalonate
339 pathway gene expression by looking at the SREBPs. There are three SREBP proteins
340 in cells produced from the genes *Srebf1* and *Srebf2* (SREBP-1a, SREBP-1c, and
341 SREBP2). These proteins are usually maintained as inactive precursors in the ER, but
342 upon appropriate signaling of a requirement for increased lipogenesis are trafficked to
343 the Golgi to be cleaved, releasing the active form of the protein that can migrate to the
344 nucleus and activate genes associated with sterol and fatty acid synthesis. Transport of
345 the SREBPs from the ER to the Golgi is regulated by the actions of SREBP cleavage
346 activating protein (SCAP). We validated siRNA sequences to target each of these three
347 genes, three for *Srebf1* and two for each of *Srebf2* and *Scap* by transfection into A549-
348 ACE2 cells for 72 h prior to treatment with DMSO for 24 h prior to collection for qRT-
349 PCR for each of the siRNA targets and the same three mevalonate pathway genes as
350 used in Fig. 3 (Fig. 4A-C).
351
352 As shown in Fig. 4A-C, the siRNAs for each gene caused varying levels of knockdown
353 for each of the target genes in DMSO conditions, but all were effective (white bars in
354 each panel). For *SCAP*, siRNA sequence 1 and 2 caused a relative level of expression

355 of 24% and 6%, respectively, compared to scrambled siRNA with DMSO. *Srebf1* had a
356 relative expression of 33, 47 and 48% for the three siRNAs, while *Srebf2* had a relative
357 level of expression at 11% and 29% for siRNA sequence 1 and 2, respectively. The loss
358 of each of these genes has some impact on the expression of mevalonate genes at
359 baseline levels since there are minor alterations in MVD, MSMO1, and FDPS
360 expression levels in DMSO conditions, but no statistically significant changes (Fig. 4A-
361 C). As described previously, to analyze the role of each gene in the UMB18-mediated
362 increase in mevalonate pathway genes, the ΔΔCT was calculated and plotted as
363 relative fold change compared to Scr/DMSO (Fig. 4D-F). UMB18 treatment of siScr cells
364 resulted in approximately a 2- and 12-fold increase in each of the three mevalonate
365 pathway genes, similar to data from previous figures, but it does not appear to alter
366 expression of either of the SREBPs nor SCAP (Fig. 4D-F).
367
368 However, when cells were transfected with siRNAs targeting *SCAP*, the fold changes in
369 expression of *MVD*, *FDPS*, and *MSMO1* from UMB18 treatment were all minimally
370 changed to Scr/DMSO (Fig. 4D). There are significant differences in the fold change
371 between the UMB18 treated siScr transfected cells and the si*SCAP* transfected cells,
372 with siRNA-1 giving significant difference for all three genes and siRNA-2 giving
373 significant differnces for *FDPS* (Fig. 4D). This suggested that the loss of SCAP
374 attenuated the impact of UMB18 treatment. When the fold change between UMB18
375 treated siScr and si*SCAP* was analyzed there was a greater than 50% drop in the
376 impact from UMB18 treatment (Fig. 4G). SREBP2 is generally considered the main
377 regulator for cholesterol synthesis genes, but SREBP1 can also regulate this pathway.

378 Our results suggest that loss of SREBP2 does not have as large of an effect on UMB18-
379 mediated increases in mevalonate pathway genes, with the fold change in Fig. 4H being
380 close to 1 when comparing UMB18 in siScr and si*SREBF2*. However, knockdown of
381 *SREBF1* caused attenuation of the UMB18-mediated increases similarly to *SCAP*,
382 again, with varying diegrees of significance seen (Fig. 4F). Overall, these data point
383 towards SCAP and SREBP1 being the main regulators of the increase in mevalonate
384 pathway genes following UMB18 treatment of A549-ACE2 cells, with SREBP2 having a
385 comparatively more minor role.
386
387 **Increased cellular cholesterol is required for UMB18-mediated antiviral activity.**
388 We have found that UMB18 caused an increase in mevalonate pathway gene
389 expression and that the canonical signaling pathway mediated by SCAP and SREBPs is
390 involved. This transcriptional response increased total cellular cholesterol, leading to the
391 question of whether the increase in cholesterol is important for antiviral activity. To
392 investigate this, we again used siRNA to target SCAP and the SREBP genes and
393 treated cells with UMB18 while also infecting with SARS-CoV-2. A549-ACE2 cells were
394 plated and transfected for 72 h as in other experiments and then were infected with
395 SARS-CoV-2 at MOI 0.1 and treated with 10μM UMB18 or 0.1% DMSO for 24 h.
396 Supernatant was collected, and viral titer determined by plaque assay on VeroE6 cells
397 expressing transmembrane protease serine 2 (TMPRSS2). With scrambled siRNA there
398 is approximately a 10-fold drop in viral titer (Fig. 5A-C), similar to the effects we
399 previously published(1). However, when *Srebf1* was knocked down by siRNA, UMB18
400 lowered viral titer by 1.23-2-fold, compared to DMSO (Fig. 5C), suggesting SREBP1 is

401 involved in UMB18-mediated antiviral activity. For *Srebf2* siRNA, one sequence
402 demonstrated a 2-fold inhibition with UMB18, while the other sequence had less effect
403 at a 7.5-fold decrease and the SCAP siRNAs were at 4.3- and 2.9-fold decrease in viral
404 titer (Fig. 5C). In all cases, viral titer inhibition due to UMB18 is attenuated by loss of the
405 SREBPs and SCAP, with varying degrees of significance. Since the loss of these genes
406 causes a decrease in mevalonate pathway gene expression induced by UMB18 (Fig. 4),
407 these data collectively suggest that increased cellular cholesterol plays a role in
408 UMB18-mediated antiviral activity.
409
410 UMB18 appears to be exerting antiviral activity through increasing expression of genes
411 involved in the mevalonate pathway. In previously described experiments, we found that
412 culturing cells in serum-free media produced a similar increase in gene expression as
413 UMB18. We therefore investigated whether viral replication was attenuated in serum-
414 free media, regardless of UMB18 treatment. A549-ACE2 cells were infected with SARS-
415 CoV-2 at MOI 0.1 in serum-free or serum-containing media with 10μM UMB18 or 0.1%
416 DMSO for 24 h prior to collection of supernatant and titration by plaque assay. UMB18
417 is equally effective at inhibiting viral replication regardless of the presence of serum
418 (Sup Fig. 1C). In serum-free media with DMSO there is a significant drop in viral
419 replication compared to serum-containing media suggesting that the increased
420 expression of mevalonate pathway genes may impact replication (Fig. S1C). The
421 inhibition is not as pronounced as UMB18 treatment and we speculate that this may be
422 a temporal effect with UMB18 causing a more rapid increase in expression of the
423 genes.

424

425 We also investigated the effects of methyl-β cyclodextrin (MβCD), a chemical that
426 extracts cholesterol from cells, to see if this would disrupt UMB18 antiviral activity.
427 Initially, A549-ACE2 cells were treated with a range of concentrations between 39 and
428 5000 µg/ml to investigate toxicity. The higher concentrations resulted in cell death based
429 on automated counting of nuclei in a 96-well plate format (Fig. 5D). At 625 µg/ml and
430 lower, there were no signs of toxicity. A549-ACE2 cells were then infected with SARS-
431 CoV-2 at MOI 3 and treated with MβCD at non-cytotoxic concentrations. At 24 hours
432 post-infection cells were fixed and immunofluorescent labeled for the viral N protein and
433 high content imaged to determine the percentage infection. Fig. 5E demonstrates that
434 MβCD has some level of antiviral activity with 625, 312.5, and 156.25 µg/ml causing
435 roughly 30-40% fewer infected cells compared to DMSO-treated cells. However, at 39
436 µg/ml, there was no antiviral activity from MβCD alone. We, therefore, combined 39
437 µg/ml MβCD with 10µM UMB18 to investigate whether extracting cholesterol from cells
438 treated with UMB18 would reduce the antiviral activity. Fig. 5F demonstrates that
439 UMB18 is a potent inhibitor infection reducing percentage infection of cells by about
440 90% compared to DMSO-treated control cells. When combined with MβCD, the
441 percentage inhibition is approximately 40%, demonstrating that MβCD significantly
442 reduced the antiviral activity of UMB18. In sum, these data suggest that reducing the
443 increase in mevalonate pathway genes with siRNA to *Srebf* genes or *SCAP*, or by
444 treating cells with a cholesterol extracting chemical both significantly reduce the antiviral
445 activity of UMB18, pointing towards cholesterol playing a role in the antiviral mechanism
446 of our chemical compound.

447

448 # Discussion

449 Building upon our identification of the SKI complex as a potential host-directed antiviral
450 drug target(1), here we have further investigated the mechanism of action of our lead
451 compound UMB18. The SKI complex is a cytosolic RNA helicase comprising SKIC2,
452 SKIC3, and SKIC8 (SKIC2 being the enzymatic core) that is a cofactor for the cytosolic
453 RNA exosome that drives 3' to 5' RNA degradation(4–6). Our previous study
454 demonstrated the SKI complex is a proviral factor as depletion of its component parts
455 reduced replication of influenza A virus (IAV) and Middle East respiratory syndrome
456 coronavirus (MERS-CoV). Using an *in silico* modeling approach we developed chemical
457 compounds that had broad spectrum antiviral activity. These chemicals were modeled to
458 target the SKI complex at the interface between the structural units SKIC3 and SKIC8,
459 with the binding pocket on SKIC8. Various chemical scaffolds were found to be antiviral,
460 and that activity was against pathogenic human coronaviruses (SARS-CoV, SARS-CoV-
461 2, and MERS-CoV), IAV, and the filoviruses Ebola and Marburg viruses. In that study,
462 we demonstrated UMB18 minimally impacts IAV entry yet potently inhbited RNA and
463 subsequent protein production to cause antiviral activity. However, beyond this
464 explanation for inhibiting viral replication, we did not further characterize the mechanism
465 of antiviral activity. Here, we identify that the antiviral activity of UMB18 is mediated by
466 an increase in cellular cholesterol.

467

468 We initially used RNA transcriptomics that were validated by qRT-PCR to demonstrate
469 that UMB18 treatment, regardless of SARS-CoV-2 infection status, caused significant

470 upregulation of genes involved in cholesterol synthesis and the mevalonate pathway
471 (Fig. 1 and 2). In agreement with the increased gene expression, we found total cellular
472 cholesterol to be increased (Fig. 2). Interestingly, these results were in the context of
473 serum supplementation and therefore cholesterol containing media which can inhibit
474 activation of the mevalonate pathway through a negative feedback loop. We found that
475 cells cultured in serum-free media activated the mevalonate pathway and addition of
476 UMB18 had minimal additive effect, suggesting the pathway was not activated further
477 (Fig. S1A and S1B). We propose that the lack of increase results from the pathway
478 already being activate and UMB18 cannot further increase signaling, however, we
479 cannot rule out alternative hypotheses that UMB18 may be modified by components of
480 serum or may not be effectively taken into cells in the absence of serum, or may have
481 impacts on roles adjact to the mevalonate pathway such as protein prenylation. We do
482 suspect either of these may to some extent play a role since virus replication is
483 attenuated in serum-free media but UMB18 still provides a greater level of inhibition
484 (Fig. S1C). As this compound is further developed, biochemical experiments to look at
485 the impact of serum will be performed.
486
487 Using surface plasmon resonance we demonstrated that UMB18 is indeed binding to *in*
488 *vitro* expressed SKIC8 and if the SKI complex is depleted by siRNA the impact of
489 UMB18 to increase genes in the mevalonate pathway is attenuated (Fig. 3), suggesting
490 specificity to the SKI complex. Although we cannot rule out the possibility of UMB18
491 interacting with other targets, we take the *in vitro* binding data combined with the
492 diminished effect of UMB18 when SKI genes were depleted to support direct and

493 specific action on the complex. We note that the loss of effect from UMB18 when each
494 individual SKI gene was knocked down was small, reaching roughly a 40% decrease
495 from depletion of SKIC8 as the most effective. We attempted to perform double or triple
496 knockdown of the genes to improve these results but could not produce reliable data
497 owing to cytopathic effect in these experiments. However, overall, these results suggest
498 that UMB18 is specifically targeting the SKI complex and increasing mevalonate gene
499 expression that causes an elevation of total cellular cholesterol.
500
501 To investigate how targeting the SKI complex with UMB18 causes an increase in
502 cholesterol synthesis we focused on the SREBPs and their regulator SCAP, which are
503 master regulators of sterol and fatty acid synthesis(13). Using siRNA, we knocked down
504 each of *Srebf1*, *Srebf2,* and *SCAP* individually and then treated cells with UMB18.
505 Depletion of any of these three genes resulted in an attenuation of UMB18-induced
506 upregulation of mevalonate pathway genes, indicating that UMB18's effect is through
507 this canonical signaling pathway (Fig. 4). Crucially, the antiviral activity of UMB18
508 against SARS-CoV-2 was markedly decrease when the SREBP or SCAP genes were
509 depleted from cells, arguing that the increased expression of mevalonate pathway
510 genes is essential to the mechanism of antiviral activity (Fig 5). Consistently, extraction
511 of cellular cholesterol using MβCD also attenuated the antiviral activity of UMB18,
512 reinforcing the importance of increased cellular cholesterol in mediating antiviral activity
513 (Fig. 5).
514

515 Our findings collectively reveal that UMB18 binds the SKI complex and activates
516 SREBP-mediated gene expression, leading to an increase in cellular cholesterol which
517 is crucial for antiviral efficacy of the compound. We have shown that UMB18 and similar
518 SKI-targeting compounds exhibit broad-spectrum activity against enveloped viruses,
519 including coronaviruses, orthomyxoviruses, and filoviruses(1), all of which rely on
520 manipulation of cellular membranes for efficient replication. We hypothesize that
521 UMB18-mediated increase in total cellular cholesterol, which causes an increase in
522 membrane rigidity, impedes the ability of these viruses to manipulate membranes and
523 thus disrupts efficient replication. Previous studies have suggested SARS-CoV-2
524 infection may downregulate expression of mevalonate pathway genes associated with
525 cholesterol synthesis(22,23). It would therefore be reasonable to hypothesize that
526 increasing expression of these genes would have antiviral activity, in alignment with our
527 data. However, contrasting studies have suggested that SARS-CoV-2 and other
528 coronaviruses cause an increase in lipid metabolism, mediated by the SREBPs, which
529 may make our results seem counter-intuitive(24–26). We propose that there may be a
530 delicate equilibrium in cholesterol levels, or a “Goldilocks” range of cellular cholesterol
531 necessary to support viral replication; deviations from this balance, whether through
532 insufficient or excessive cholesterol disrupts membrane dynamics and adversely affects
533 viral replication. Indeed, our data somewhat support this notion that a delicate balance
534 of cholesterol is important and both an increase and decrease in cellular cholesterol can
535 impact viral replication from our data showing that MβCD, which extracts cellular
536 cholesterol, has antiviral activity (Fig. 5E).
537

538 Our results are looking at cellular level changes in cholesterol synthesis, rather than the
539 context of a high cholesterol organism. It has been suggested that lowered cellular
540 cholesterol can be antiviral(27,28). But, again, based on our data we suggest there may
541 be a delicate balance and the disruption of cellular cholesterol either to increase or
542 decrease can be detrimental to SARS-CoV-2 replication. It is worth noting that many
543 studies have implicated high cholesterol with increased COVID-19 severity. We do not
544 think these necessarily impact the potential efficacy of our development antiviral though
545 since the increased cholesterol seen in humans usually comes from, or with various
546 other underlying health conditions which can all impact viral disease pathogenesis. In
547 future work we intend to further study the role these cellular changes have at an
548 organismal level using animal models of UMB18 treatment.
549
550 One hypothesis for the mechanism through which UMB18 is causing the SREBP-
551 mediated transcriptional changes draws from work by Yang *et al.*(21), which linked
552 SKIC2 deletion in mice to an increase in mTORC1 signaling. Despite efforts to assess
553 whether UMB18 activated mTORC1 as assess by phosphorylation levels of S6K1, we
554 observed no significant changes (Fig. S2). The activation of mTORC1 drives many
555 cellular changes, one of which is the activation of the SREBP proteins, and thus a link
556 between the SKI complex and mTORC1 activation could make sense in the context of
557 our data. It is possible that UMB18 could activate mTORC1 but not at a level to observe
558 changes to the phosphorylation status of S6K1.
559

560 Alternatively, UMB18 may alter the activity of the SKI complex as an RNA helicase and
561 impact genes that regulate SREBP proteins independently of mTORC1. For instance,
562 the SKI complex has been shown to have a role in resolution of stalled ribosomes(29)
563 which could be hypothesized to be disrupted by treatment with UMB18. Stalled
564 ribosomes can activate ZAKα, which can in turn activate JNK signaling(30) and JNK
565 signaling has been linked to activation of SREBPs(31). Future research will explore the
566 interaction between UMB18, the SKI complex and these various cellular signaling
567 pathways.
568
569 Notably, our findings demonstrate that *Srebf1* knockdown appeared to more potently
570 attenuate the antiviral activity of UMB18 compared to *Srebf2*. It is generally considered
571 that SREBP2 is primarily involved in expression of genes in the cholesterol synthesis
572 pathway, while SREBP1 predominantly influences fatty acid synthesis genes(16,17).
573 However, there are two isoforms of SREBP1 generated from alternative start sites,
574 SREBP1a and SREBP1c(15). Studies have suggested that SREBP1a can play roles in
575 promoting expression of genes involved in cholesterol synthesis, along with lipogenic
576 genes(16). Thus, our data may point towards a nuanced interaction between the SKI
577 complex and SREBP activation, warranting further research into how SREBP isoforms
578 contribute to cholesterol regulation and the antiviral activity of UMB18.
579
580 This study advances our understanding of our developmental host-directed, broad-
581 spectrum antiviral therapeutic targeting the SKI complex. Building on our previous work
582 which established the SKI complex as a host-directed target to inhibit diverse highly

583 pathogenic human viruses, we reveal a crucial role for increased cellular cholesterol in
584 mediating this antiviral effect. Our findings prompt further investigation into the
585 mechanisms by which the SKI complex, an RNA helicase associated with 3' to 5' RNA
586 degradation, influences metabolic pathways crucial for lipid and cholesterol synthesis, a
587 finding that will be the focus of future work.
588

589 Material and Methods

590 **Mammalian cell culture**

591 A549 cells and A549 cells overexpressing human ACE2 (A549-ACE2, kindly provided
592 by Dr. Brad Rosenberg (MSSM, NYC)) were cultured in DMEM (Quality Biologicals),
593 supplemented with 10% (v/v) heat inactivated fetal bovine serum (FBS; Sigma) and 1%
594 (v/v) penicillin/streptomycin (pen/strep, 10,000 U/ml / 10 mg/ml; Gemini Bio-Products).
595 VeroE6 cells overexpressing TMPRSS2 (VeroT, kindly provided by Shutoku Matsuyama
596 (National Institute of Infectious Diseases, Japan - Shirato2018_Virology) were cultured
597 in DMEM, supplemented with 10% FBS, 1% pen/strep and 1% (v/v) L-glutamine (2 mM
598 final concentration, Gibco). Cells were maintained at 37°C and 5% CO_2.
599

600 **Chemical compounds**

601 SKI targeting compounds were synthesized by, and purchased from, Dalriada Drug
602 Discovery and were previously described(1). Methyl-beta-cyclodextrin (MβCD) was
603 purchased from Sigma.
604

605 **Viruses and infections**

606 Details on stock production have been described previously(1). SARS-CoV-2 strain
607 Washington 1 (WA1) was initially provided by the CDC (BEI #NR-52281). All
608 coronavirus work was performed in a Biosafety Level 3 laboratory and approved by our
609 Institutional Biosafety Committee. In all cases of infection for experiments, cells were
610 plated one day prior to infection to be at a desired confluence for infection. All viral titer
611 were determined using plaque assays on VeroT cells as described(32). For
612 experimental infections, virus was diluted to indicated MOI in media used for culture of
613 A549 cells with addition of chemical compounds or controls as appropriate. For
614 experiments using MβCD, 50 mM Hepes (Gibco) was additionally added to the media.
615

616 **RNA extraction and qRT-PCR**

617 RNA extractions and cDNA reactions were performed as described previously(1) using
618 Direct-zol RNA miniprep kit (Zymo Reserach) and RevertAid RT Kit (Thermo Scientific).
619 The primers used are listed in the table below. A QuantStudio 5 (Applied Biosystems)
620 was used for the qRT-PCR reactions. Loading was normalized using GAPDH and fold
621 change was determined by calculating ΔΔCT after normalization.

622 <u>RT-PCR primers</u>

623 All primers for qRT-PCR were purchased from Integrated DNA Technologies (IDT) using
624 their pre-designed qPCR assay primers:

Gene target	**IDT Assay ID**
SKIC2 (A.K.A SKIV2L)	Hs.PT.58.14722008
SKIC3 (A.K.A TTC37)	Hs.PT.58.26762302
SKIC8 (A.K.A WDR61)	Hs.PT.58.157001
HMGCS1	Hs.PT.58.4084870

HMGCR	Hs.PT.58.41105491
MVK	Hs.PT.58.40379926
MVD	Hs.PT.58.39035173
IDI1	Hs.PT.58.1930362
FDPS	Hs.PT.58.27570524
MSMO1	Hs.PT.58.3747602
SCAP	Hs.PT.58.45442299
SREBF1	Hs.PT.58.3359761
SREBF2	Hs.PT.58.45335433
GAPDH	Hs.PT.39a.22214836

625

626

627 **Transcriptomic sequencing and analysis**

628 Library preparation and sequencing were carried out by the University of Maryland
629 Institute of Genomic Sciences (IGS; Baltimore, MD, USA) on an Illumina NovaSeq
630 6000; 100bp paired-end sequencing on an S4 flow cell (Illumina, San Diego, CA, USA).
631 Reads were preprocessed using cutadapt v3.4(33), then aligned to the *Mus musculus*
632 genome (assembly GRCm38) with STAR v2.7.8(34). Gene expression analysis was
633 carried out using DESeq2 v4.1.0(35) in R (Rstudio, Boston, MA, USA). Pathway
634 analysis was carried out using Ingenuity Pathway Analysis (QIAGEN, Hilden, Germany)
635 using an alpha value of $p_{adj} < 0.01$ to call a gene significantly differentially expressed.
636 Raw sequence data is available in the NCBI Sequence Read Archive under the
637 accession number PRJNA1055076.

638

639 **Mass spectrometry imaging**

640 A modified cell culture apparatus was used for compatibility with mass spectrometry
641 imaging (MSI). Briefly, Superfrost plus gold microscope slides were autoclaved with
642 flexible silicon 12-well transwell adapters (Flexiperm, Starstedt), dried completely, and
643 the transwell adapters mounted. Wells were coated with 0.1 mg/mL poly-l-lysine (0.1 M
644 borate buffer pH 8.5) overnight at 37°C, aspirated, and dried. Cells were grown in the
645 transwells overnight and subsequently treated with 10μM UB18 or 0.1% DMSO for 24h.
646 At the end of the incubation, supernatants were aspirated, the transwell mount was
647 removed, and the slides were submerged in ice-cold 50 mM ammonium formate (pH
648 6.7) for 1 minute with gentle rocking. Excess buffer was removed by tilting and using
649 absorbent paper. Slides were dried, flat, in a desiccator for 20 minutes. Silver-assisted
650 laser desorption ionization (Ag-LDI) was used to ionize cholesterol on a quadropole time
651 of flight (qTOF) mass spectrometer in imaging mode (Yang2020_JMassSpectrom).
652 Silver nitrate (8.5 mg/mL in 0.1% trifluoroacetic acid/methanol) was sprayed on the
653 slides using an HTX M5 Matrix Sprayer with the following settings: 45°C nozzle, 40 mm
654 height, 24 passes, 0.075 mL/min flow, 500 mm/min speed, 4 mm track spacing, 20 psi,
655 2 L/min N2, in “CC” pattern, with 0 s dry time between passes. Cholesterol imaging data
656 were captured from an area of uniform monolayer (>80% confluence) integrity guided by
657 an optical pre-scan using a Bruker Daltonics timsTOF Flex (Billerica, MA) in positive ion
658 mode with a 50 μM scan area (11 μM x 11 μM beamscan), over range *m/z* 100-1000
659 with enhanced quadratic fit calibration to Agilent Tune-Mix, 500 shots per pixel at 10 kHz
660 with 5-point setting in M5 small laser focus. Total scan area per sample was ~3 mm^2
661 resulting in ~1200 pixels per replicate, with quadruplicate samples per condition. Data
662 analyzed in SCiLS Lab (Bruker Daltonics), normalized (total ion current), projected with

663 hotspotting on, and visualized as the ion *m/z* 493.260 +/-2.2 mDa ([cholesterol+Ag_{107}]$^+$)
664 ion; the [cholesterol+Ag_{109}]$^+$ ion data was in agreement. Student's T-test and a receiver-
665 operator characteristic were performed between vehicle-treated and UMB18-treated
666 cells on quadruplicate samples.
667
668 **Expression and purification of SKIC8**
669 Transformed *E. coli* BL21 (DE3) cells containing the full-length human *SKIC8* gene with
670 a HisX6 tag in the pET-28a(+) vector were grown in Luria-Bertani (LB)-Kanamycin broth
671 at 37ºC until the optical density at 600 nm equaled 0.8. SKIC8 protein expression was
672 induced with 1 mM Isopropyl β-D-1-thiogalactopyranoside for 20 h at 15°C. Cells were
673 lysed using Bugbuster (Novagen) supplemented with protease and phosphatase
674 inhibitors (Thermo Scientific). Lysates were clarified by centrifugation at 14,000 rpm for
675 30 min. and the supernatant was applied to a Talon Metal Affinity Resin (Clontech)
676 column equilibrated in 50 mM sodium phosphate (pH 7.8) containing 10 mM imidazole
677 and 300 mM NaCl. The column was washed with the same sodium phosphate buffer
678 containing 20 mM imidazole. SKIC8 was eluted in 50 mM sodium phosphate (pH 7.8)
679 containing a 50-250 mM imidazole gradient and 300 mM NaCl. The fractions containing
680 SKIC8, as determined following SDS-PAGE, were pooled, and concentrated with an
681 Amicon ultrafiltration cell (Millipore, Bedford, MA). The concentrated protein was
682 dialyzed against 20 mM Tris-HCl (pH 7.8) containing 150 mM NaCl.
683
684 **Surface Plasmon Resonance (SPR)**

685 SKIC8 and test compound interactions were evaluated using a Biacore T-200
686 instrument (GE Healthcare). A carboxymethylated dextran chip (CM5, GE Healthcare)
687 was used to immobilize SKIC8. A net positive charge is required for direct amine
688 coupling; therefore, the proteins were diluted to a final concentration of 30 µg/ml in 10
689 mM sodium acetate buffer pH 4.0. The protein was injected at 2 µl/min until
690 approximately a 4500 resonance/response unit level of immobilized SKIC8 was
691 reached, and then the flow cell was deactivated with 1 M ethanolamine HCl (pH 8.5).
692 Degassed 20 mM Hepes (pH 7.4) containing 5 mM MgCl2, 100 mM NaCl, and 0.005%
693 Nonidet P40 was utilized as continuous running buffer for all experiments. Test
694 compound binding interactions with SKIC8 were investigated by injecting test compound
695 (1.0 –50 µM) at a flow rate of 20 µl/min. The resulting sensorgrams were analyzed using
696 BIAevaluation 3.1 software (GE Healthcare) to determine the dissociation constant (K_D)
697 as previously described(36).
698
699 **RNAi knockdown**
700 Cells were seeded to 24-well plates at a density of 4.4e4 cells/well one day prior to
701 transfection. Transfections were performed using Oligofectamine (Thermo Scientific) to
702 the manufacture's methods. Briefly, per well of transfection, 4.4µl Opti-MEM (Gibco) was
703 mixed with 2.2µl Oligofectamine and incubated at room temperature (RT°C) for 5 min,
704 while 35.5µl Opti-MEM was mixed with 0.8µl 50mM siRNA in a separate tube. The two
705 tubes were combined and incubated at RT°C for 20 minutes prior to addition of 177µl
706 Opti-MEM. Cells were washed 1x with PBS and 1x with OptiMEM then 200µl of
707 transfection mixture was added per well. All siRNAs were purchased from Sigma using

708 their Rosetta prediction system for predesigned sequences. MISSION siRNA Universal
709 Negative Control #1 (Sigma) was used as the scrambled control sequence. Sequences
710 are displayed in table:

711 RNAi sequences

Gene name	siRNA ID
SKIC2 (A.K.A SKIV2L)	SASI_Hs01_00196881
SKIC3 (A.K.A TTC37)	SASI_Hs01_00010354
SKIC8 (A.K.A WDR61)	SASI_Hs01_00155941
SCAP si-1	SASI_Hs01_00032110
SCAP si-2	SASI_Hs01_00032111
SREBF1 si-1	SASI_Hs01_00051828
SREBF1 si-2	SASI_Hs01_00051829
SREBF2 si-1	SASI_Hs01_00075424
SREBF2 si-2	SASI_Hs01_00075425
SREBF2 si-3	SASI_Hs01_00075426

712

713 **Western blotting**

714 Whole cell lysates were made using Triton-X100 (Tx100) lysis buffer lysis buffer (1%
715 Tx100 (v/v), 150mM NaCl , 50mM Tris (all Sigma), pH8). In all cases 1x cOmplete Mini,
716 EDTA-Free protease inhibitor cocktail (Roche) was added to the lysis buffer and for
717 experiments involving S6K and phospho-S6K (pS6K), Phosphatase Inhibitor Cocktail 2
718 (Sigma) was additionally used. Western blotting procedures have been previously
719 described(37). Primary antibodies used as follows: p70 S6K (Cell Signaling

720 Technologies #9202S, 1:1000 dilution), phospho-p70 S6K (T421/S424) (Cell Signaling
721 Technologies #9204S, 1:1000 dilution) and mouse anti-tubulin (clone DMA1A, Sigma,
722 1:1000). Secondary antibodies were used as follows: goat anti-rabbit HRP and goat
723 anti-mouse HRP (both 0.8 mg/ml, Thermo Scientific, 1:10,000 diluted) which were
724 detected using ECL Prime (Amersham).
725
726 **Data analysis**
727 All graphs produced and statistical analyese performed using GraphPad Prism 10.3
728 software.
729

730 Acknowledgements

731 Acknowledgments: We thank We would like to thank all of the Frieman, Jackson and
732 Coughlan lab members for their help in this study.

733 Funding: MBF is supported by an endowment from The Alicia and Yaya Foundation.
734 The funders had no role in study design, data collection and analysis, decision to
735 publish, or preparation of the manuscript.

736

737 References

738 1. Weston S, Baracco L, Keller C, Matthews K, McGrath ME, Logue J, et al. The SKI
739 complex is a broad-spectrum, host-directed antiviral drug target for coronaviruses,
740 influenza, and filoviruses. Proc Natl Acad Sci U S A. 2020 Dec 1;117(48):30687–98.

741 2. Cox M, Peacock TP, Harvey WT, Hughes J, Wright DW, Willett BJ, et al. SARS-CoV-
742 2 variant evasion of monoclonal antibodies based on in vitro studies. Nat Rev
743 Microbiol. 2023 Feb;21(2):112–24.

744 3. Sanderson T, Hisner R, Donovan-Banfield I, Hartman H, Løchen A, Peacock TP, et
745 al. A molnupiravir-associated mutational signature in global SARS-CoV-2 genomes.
746 Nature. 2023 Nov;623(7987):594–600.

747 4. Houseley J, Tollervey D. The Many Pathways of RNA Degradation. Cell. 2009 Feb
748 20;136(4):763–76.

749 5. Schneider C, Tollervey D. Looking into the barrel of the RNA exosome. Nat Struct
750 Mol Biol. 2014 Jan;21(1):17–8.

751 6. Januszyk K, Lima CD. The eukaryotic RNA exosome. Curr Opin Struct Biol. 2014
752 Feb;24:132–40.

753 7. Johnson SJ, Jackson RN. Ski2-like RNA helicase structures: common themes and
754 complex assemblies. RNA Biol. 2013 Jan;10(1):33–43.

755 8. Toh-E A, Guerry P, Wickner RB. Chromosomal superkiller mutants of
756 Saccharomyces cerevisiae. J Bacteriol. 1978 Dec;136(3):1002–7.

757 9. Widner WR, Wickner RB. Evidence that the SKI antiviral system of Saccharomyces
758 cerevisiae acts by blocking expression of viral mRNA. Mol Cell Biol. 1993
759 Jul;13(7):4331–41.

760 10. Goldstein JL, Brown MS. Regulation of the mevalonate pathway. Nature. 1990
761 Feb;343(6257):425–30.

762 11. Luo J, Yang H, Song BL. Mechanisms and regulation of cholesterol homeostasis.
763 Nat Rev Mol Cell Biol. 2020 Apr;21(4):225–45.

764 12. Cerqueira NMFSA, Oliveira EF, Gesto DS, Santos-Martins D, Moreira C, Moorthy
765 HN, et al. Cholesterol Biosynthesis: A Mechanistic Overview. Biochemistry. 2016 Oct
766 4;55(39):5483–506.

767 13. Brown MS, Goldstein JL. The SREBP Pathway: Regulation of Cholesterol
768 Metabolism by Proteolysis of a Membrane-Bound Transcription Factor. Cell. 1997
769 May 2;89(3):331–40.

770 14. Hua X, Nohturfft A, Goldstein JL, Brown MS. Sterol resistance in CHO cells traced to
771 point mutation in SREBP cleavage-activating protein. Cell. 1996 Nov 1;87(3):415–
772 26.

773 15. Shimomura I, Shimano H, Horton JD, Goldstein JL, Brown MS. Differential
774 expression of exons 1a and 1c in mRNAs for sterol regulatory element binding
775 protein-1 in human and mouse organs and cultured cells. Journal of Clinical
776 Investigation. 1997 Mar 3;99(5):838.

777 16. Horton JD, Goldstein JL, Brown MS. SREBPs: activators of the complete program of
778 cholesterol and fatty acid synthesis in the liver. J Clin Invest. 2002 May
779 1;109(9):1125–31.

780 17. Xu X, So JS, Park JG, Lee AH. Transcriptional control of hepatic lipid metabolism by
781 SREBP and ChREBP. Semin Liver Dis. 2013 Nov;33(4):301–11.

782 18. Nohturfft A, DeBose-Boyd RA, Scheek S, Goldstein JL, Brown MS. Sterols regulate
783 cycling of SREBP cleavage-activating protein (SCAP) between endoplasmic
784 reticulum and Golgi. Proceedings of the National Academy of Sciences. 1999 Sep
785 28;96(20):11235–40.

786 19. Sun LP, Li L, Goldstein JL, Brown MS. Insig required for sterol-mediated inhibition of
787 Scap/SREBP binding to COPII proteins in vitro. J Biol Chem. 2005 Jul
788 15;280(28):26483–90.

789 20. Nagoshi E, Imamoto N, Sato R, Yoneda Y. Nuclear import of sterol regulatory
790 element-binding protein-2, a basic helix-loop-helix-leucine zipper (bHLH-Zip)-
791 containing transcription factor, occurs through the direct interaction of importin beta
792 with HLH-Zip. Mol Biol Cell. 1999 Jul;10(7):2221–33.

793 21. Yang K, Han J, Asada M, Gill JG, Park JY, Sathe MN, et al. Cytoplasmic RNA quality
794 control failure engages mTORC1-mediated autoinflammatory disease. Journal of
795 Clinical Investigation. 2022 Jan 18;132(2):e146176.

796 22. Gomez Marti JL, Wells A, Brufsky AM. Dysregulation of the mevalonate pathway
797 during SARS-CoV-2 infection: An in silico study. Journal of Medical Virology.
798 2021;93(4):2396–405.

799 23. Wang X, Zhao Y, Yan F, Wang T, Sun W, Feng N, et al. Viral and Host
800 Transcriptomes in SARS-CoV-2-Infected Human Lung Cells. J Virol. 2021 Aug
801 25;95(18):e0060021.

802 24. Dias SSG, Soares VC, Ferreira AC, Sacramento CQ, Fintelman-Rodrigues N,
803 Temerozo JR, et al. Lipid droplets fuel SARS-CoV-2 replication and production of
804 inflammatory mediators. PLOS Pathogens. 2020 Dec 16;16(12):e1009127.

805 25. Gao P, Ji M, Liu X, Chen X, Liu H, Li S, et al. Apolipoprotein E mediates cell
806 resistance to influenza virus infection. Science Advances. 2022 Sep
807 21;8(38):eabm6668.

808 26. Yuan S, Chu H, Chan JFW, Ye ZW, Wen L, Yan B, et al. SREBP-dependent
809 lipidomic reprogramming as a broad-spectrum antiviral target. Nat Commun. 2019
810 Jan 10;10(1):120.

811 27. Wing PAC, Schmidt NM, Peters R, Erdmann M, Brown R, Wang H, et al. An ACAT
812 inhibitor suppresses SARS-CoV-2 replication and boosts antiviral T cell activity.
813 PLOS Pathogens. 2023 May 3;19(5):e1011323.

814 28. Wang H, Yuan Z, Pavel MA, Jablonski SM, Jablonski J, Hobson R, et al. The role of
815 high cholesterol in SARS-CoV-2 infectivity. Journal of Biological Chemistry [Internet].
816 2023 Jun 1 [cited 2024 Aug 28];299(6). Available from:
817 https://www.jbc.org/article/S0021-9258(23)01791-X/abstract

818 29. Zinoviev A, Ayupov RK, Abaeva IS, Hellen CUT, Pestova TV. Extraction of mRNA
819 from Stalled Ribosomes by the Ski Complex. Molecular Cell. 2020 Mar
820 19;77(6):1340-1349.e6.

821 30. Snieckute G, Genzor AV, Vind AC, Ryder L, Stoneley M, Chamois S, et al. Ribosome
822 stalling is a signal for metabolic regulation by the ribotoxic stress response. Cell
823 Metabolism. 2022 Dec;34(12):2036-2046.e8.

824 31. Kotzka J, Knebel B, Haas J, Kremer L, Jacob S, Hartwig S, et al. Preventing
825 Phosphorylation of Sterol Regulatory Element-Binding Protein 1a by MAP-Kinases
826 Protects Mice from Fatty Liver and Visceral Obesity. PLOS ONE. 2012 Feb
827 27;7(2):e32609.

828 32. Weston S, Coleman CM, Haupt R, Logue J, Matthews K, Li Y, et al. Broad Anti-
829 coronavirus Activity of Food and Drug Administration-Approved Drugs against
830 SARS-CoV-2 In Vitro and SARS-CoV In Vivo. J Virol. 2020 Oct 14;94(21):e01218-
831 20.

832 33. Martin M. Cutadapt removes adapter sequences from high-throughput sequencing
833 reads. EMBnet.journal. 2011 May 2;17(1):10–2.

834 34. Dobin A, Davis CA, Schlesinger F, Drenkow J, Zaleski C, Jha S, et al. STAR:
835 ultrafast universal RNA-seq aligner. Bioinformatics. 2013 Jan 1;29(1):15–21.

836 35. Love MI, Huber W, Anders S. Moderated estimation of fold change and dispersion
837 for RNA-seq data with DESeq2. Genome Biology. 2014 Dec 5;15(12):550.

838 36. Burkhard KA, Chen F, Shapiro P. Quantitative analysis of ERK2 interactions with
839 substrate proteins: roles for kinase docking domains and activity in determining
840 binding affinity. J Biol Chem. 2011 Jan 28;286(4):2477–85.

841 37. Weston S, Matthews KL, Lent R, Vlk A, Haupt R, Kingsbury T, et al. A Yeast
842 Suppressor Screen Used To Identify Mammalian SIRT1 as a Proviral Factor for
843 Middle East Respiratory Syndrome Coronavirus Replication. J Virol. 2019 Aug
844 15;93(16):e00197-19.

845

846 Author Contributions:

847 - Conceptualization: SW, MBF
848 - Data curation: LT,
849 - Formal analysis: SW, LT, AS, PS,
850 - Funding acquisition: MBF
851 - Investigation: SW, LB, AS, GK,
852 - Methodology: SW, LT, AS, PS,
853 - Resources: ADM
854 - Supervision: MBF
855 - Visualization: SW, LT, AS, PS,
856 - Writing – original draft: SW, AS, PS, MBF
857 - Writing – review & editing: SW, MFB
858

Competing Interests: The authors declare the following competing interesting: M.B.F is the lead inventor along with S.W. and A.D.M as contributing inventors for patents held for development of SKI targeting compounds (of which UMB18 is one) with antiviral activity. The patent filings were through University of Maryland, Baltimore and listed as PCT/US20/36483 and PCT/US2021/1061863. There has been a corporate partnership with Aikido Pharmaceuticals for developmental research on the compound along with others that target the SKI complex. This developmental work has not influenced the academic research presented in this paper.

Patents: Filed patents: Patents on UMB18 and related compounds have been filed through University of Maryland, Baltimore and listed as PCT/US20/36483 and PCT/US2021/1061863.

Data and Material Availability: All data needed to evaluate the conclusions in this paper are present in the paper and supplementary materials. Data are also deposited at https://osf.io/63h8t/.

Figure Legend

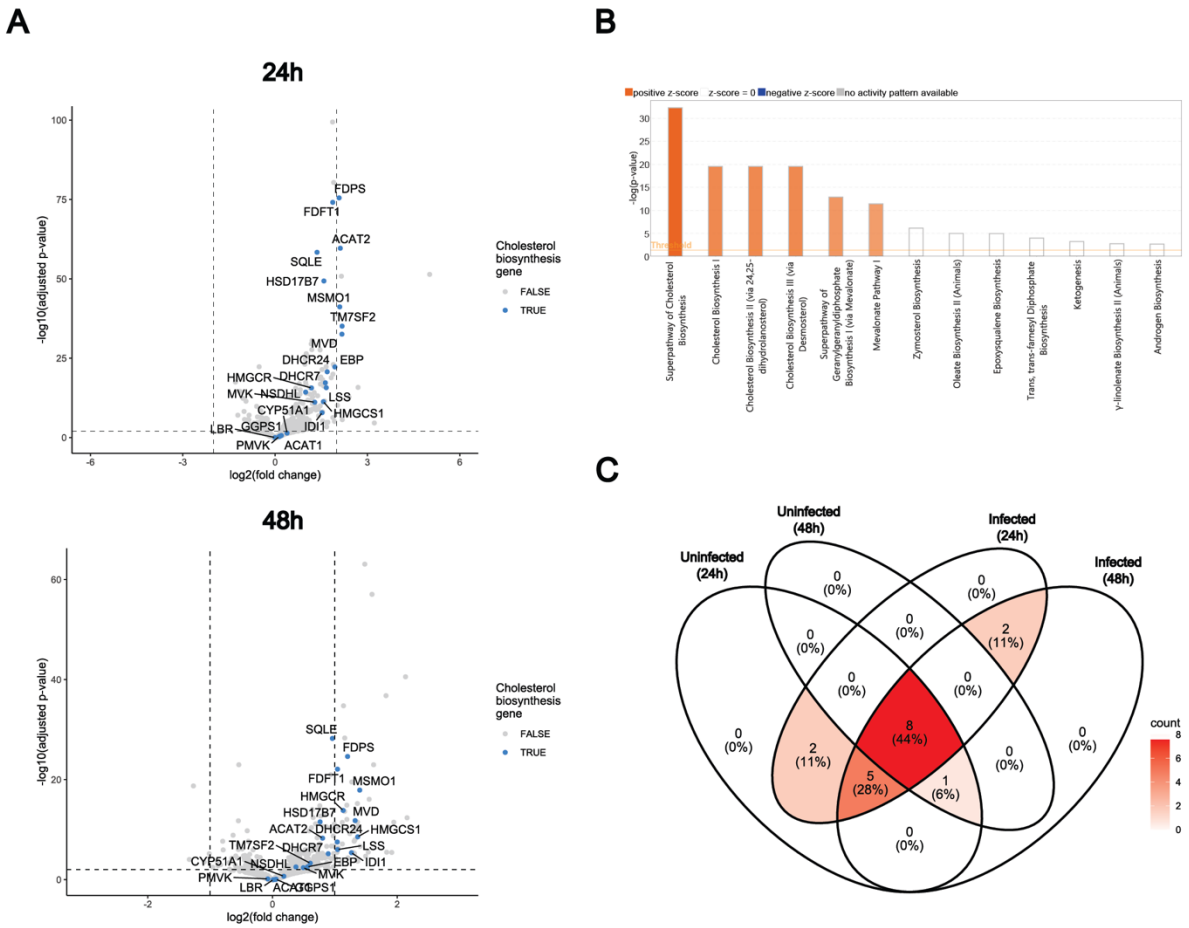

Figure 1 – Transcriptomic analysis of UMB18 treated cells.

A) Volcano plots showing differential expression of genes at 24h (top) and 48h (bottom) in uninfected A549 cells treated with UMB18 compared to untreated, uninfected A549 cells. Cholesterol biosynthesis genes are colored blue and labeled. A horizontal dashed line is drawn at p_{adj} = 0.01, vertical dashed lines are drawn at +/- 2-fold change. B) Plot showing significantly enriched pathways in uninfected A549 cells treated with UMB18 compared to untreated, uninfected A549 cells at 24h. Orange bars show pathways with predicted increased pathway output (z > 2); white bars show pathways with no predicted

activity pattern (z = 0); blue bars indicate a predicted decrease in pathway output (z < -2). C) Venn Diagram comparing upregulation of cholesterol biosynthesis genes in UMB18-treated A549 cells against timepoint- and infection-matched, untreated controls. The number and color intensity in each area corresponds to the number of cholesterol biosynthesis genes that are significantly upregulated ($p_{adj} < 0.01$).

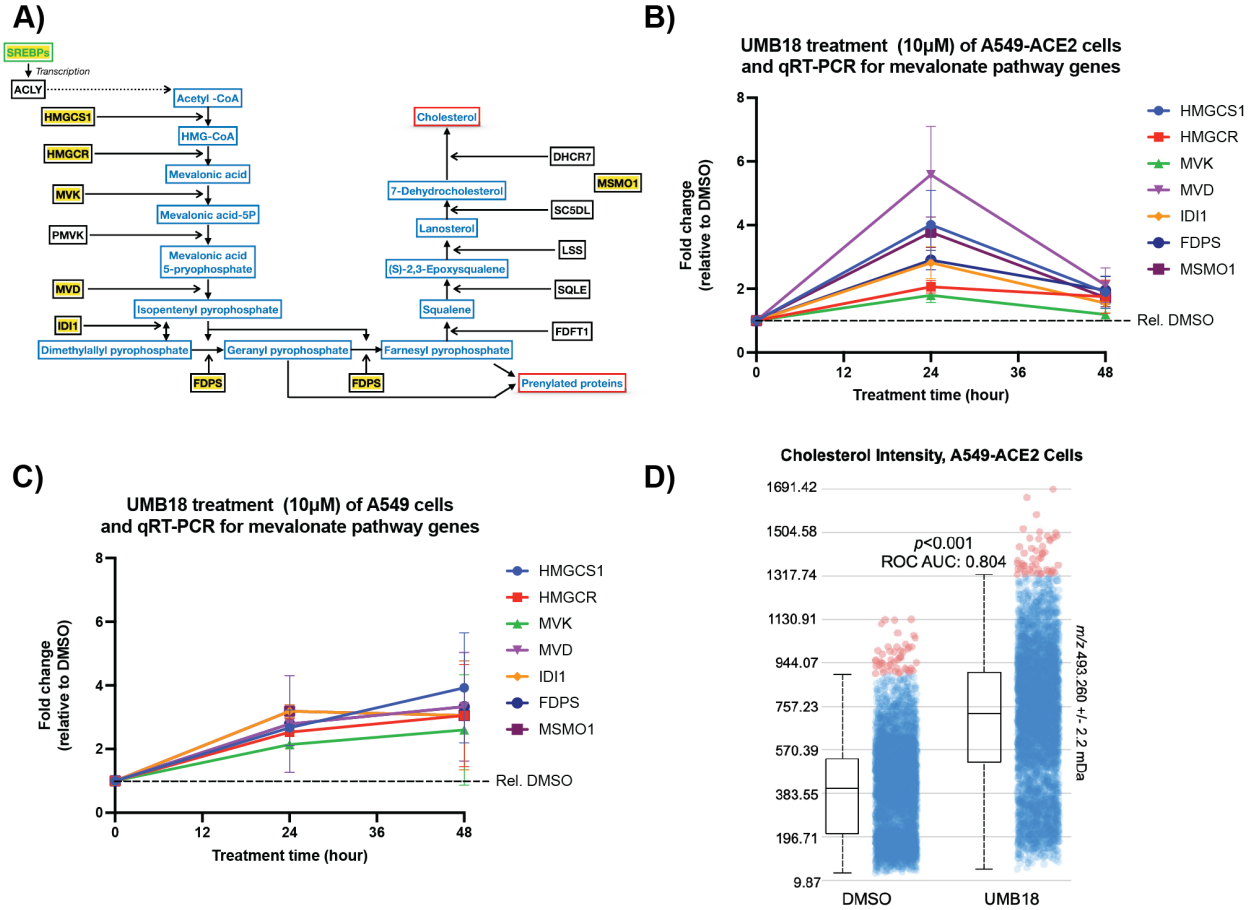

Figure 2 – UMB18 causes increased expression of mevalonate pathway genes and cellular cholesterol.

A) Schematic representation of the mevalonate pathway leading to cholesterol synthesis. In blue are metabolic products of the pathway and in black are the enzymes that regulate the various steps with those that are highlighted being analyzed by qRT-PCR through the paper. B and C) A549-ACE2 cells (B) or A549 cells (C) were treated with 10μM UMB18 or 0.1% DMSO vehicle control and collected at 24 h or 48 h in TRIzol for qRT-PCR analysis of expression of various genes throughout the mevalonate pathway. The CT values were set relative to GAPDH as a housekeeping gene control and then relative fold change calculated between UMB18 treated cells and DMSO

902 treated cells. D) Relative intensity cloud projection with box plot of *m/z* 493.260 +/- 2.2

903 mDa ([cholesterol+Ag_{107}]$^{+}$) ion per image pixel for UMB18- and DMSO-treated cells with

904 area-under-the-curve (AOC) from a receiver-operator characteristic analysis. Student's

905 T-test base on quadruplicate samples.

906

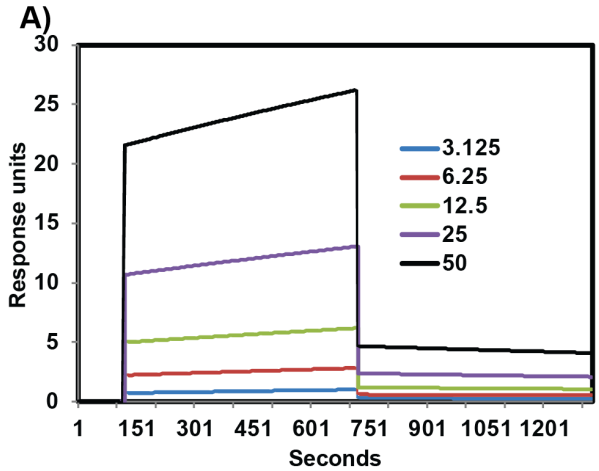

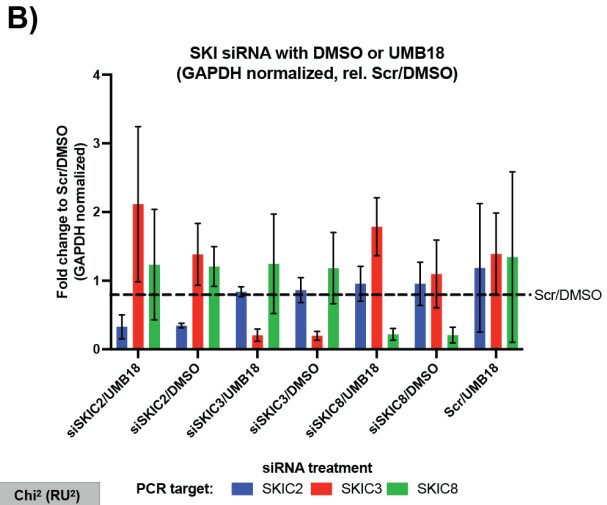

ka (1/Ms)	kd (1/s)	KD (M)	Rmax (RU)	Conc (M)	RI (RU)	Chi² (RU²)
27.1	0.002195	8.1E-05	63.81	3.13E-06	0.7169	0.309
				6.25E-06	2.224	
				1.25E-05	4.987	
				2.5E-05	10.68	
				5E-05	21.55	

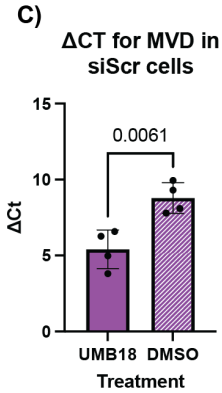

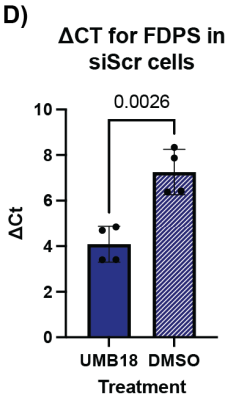

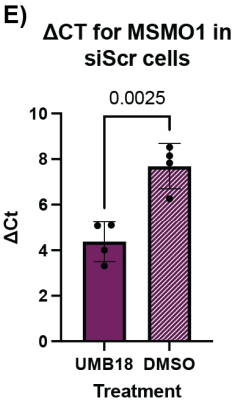

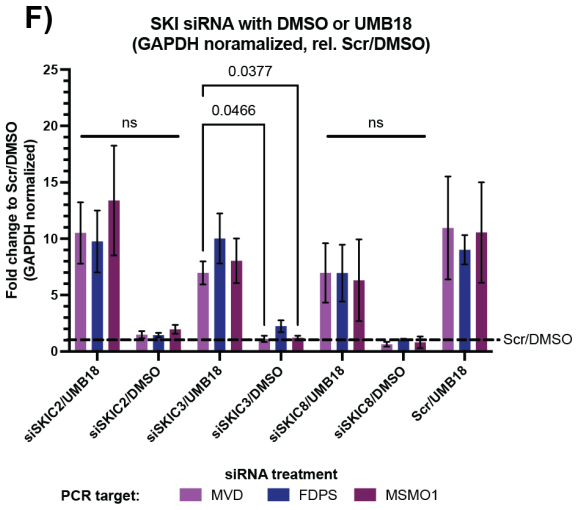

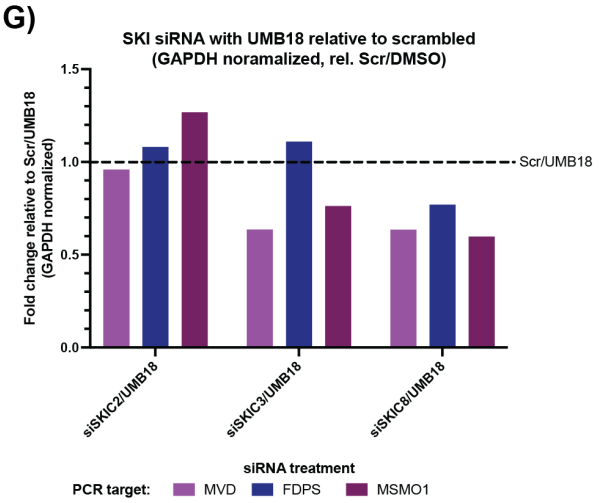

907

908 **Figure 3 – UMB18 directly binds the SKI complex and that is required for**
909 **increased cellular cholesterol.**
910 A) Binding of UMB18 to SKIC8. The binding affinity of immobilized SKIC8 to UMB18 at
911 various concentrations was quantified by SPR as described in the methods. B) A549-
912 ACE2 cells were transfected with siRNAs targeting each of the three SKI complex
913 genes (SKIC2, SKIC3, and SKIC8) for 72h prior to treatment with 10μM UMB18 or 0.1%
914 DMSO for 24 h. Cells were collected in TRIzol and qRT-PCR performed for each of the
915 three SKI genes in all of the various conditions after normalization with GAPDH.
916 Scrambled siRNA (siScr) cells treated with DMSO (siScr/DMSO) were used as the
917 control to determine relative fold change. C-E) Using the same RNA samples and qRT-
918 PCR data in B, the Ct values were normalized to GAPDH and the ΔCt values for three
919 mevalonate pathway genes (MVD, FDPS and MSMO1, respectively) from the
920 siScr/DMSO samples treated with either UMB18 or DMSO are plotted. Student's t-test
921 was performed and the p-values are labled for the comparison. F) From the same RNA
922 samples, the relative fold change for the same three mevalonate pathway genes
923 compared to siScr/DMSO in all other conditions was determined. Two-way ANOVA
924 testing was performed for all comparisons, but only the comparisons between UMB18
925 or DMSO treatment for each siRNA treatment are shown. Unless otherwise indicated,
926 there were no significant differences (ns), based on p value < 0.05. G) To further
927 analyze the impact of SKI siRNA transfection on UMB18 treatment the fold change for
928 siScr/UMB18 was set relative to the fold change in the SKI siRNA transfected cells,
929 treated with UMB18. In this comparison a fold change of 1 would mean no difference
930 between SKI siRNA and scrambled siRNA with UMB18 and a fold change below 1

931 means a lower change from UMB18 treatment in SKI siRNA. All RNA data are from two

932 experiments performed in duplicate wells.

933

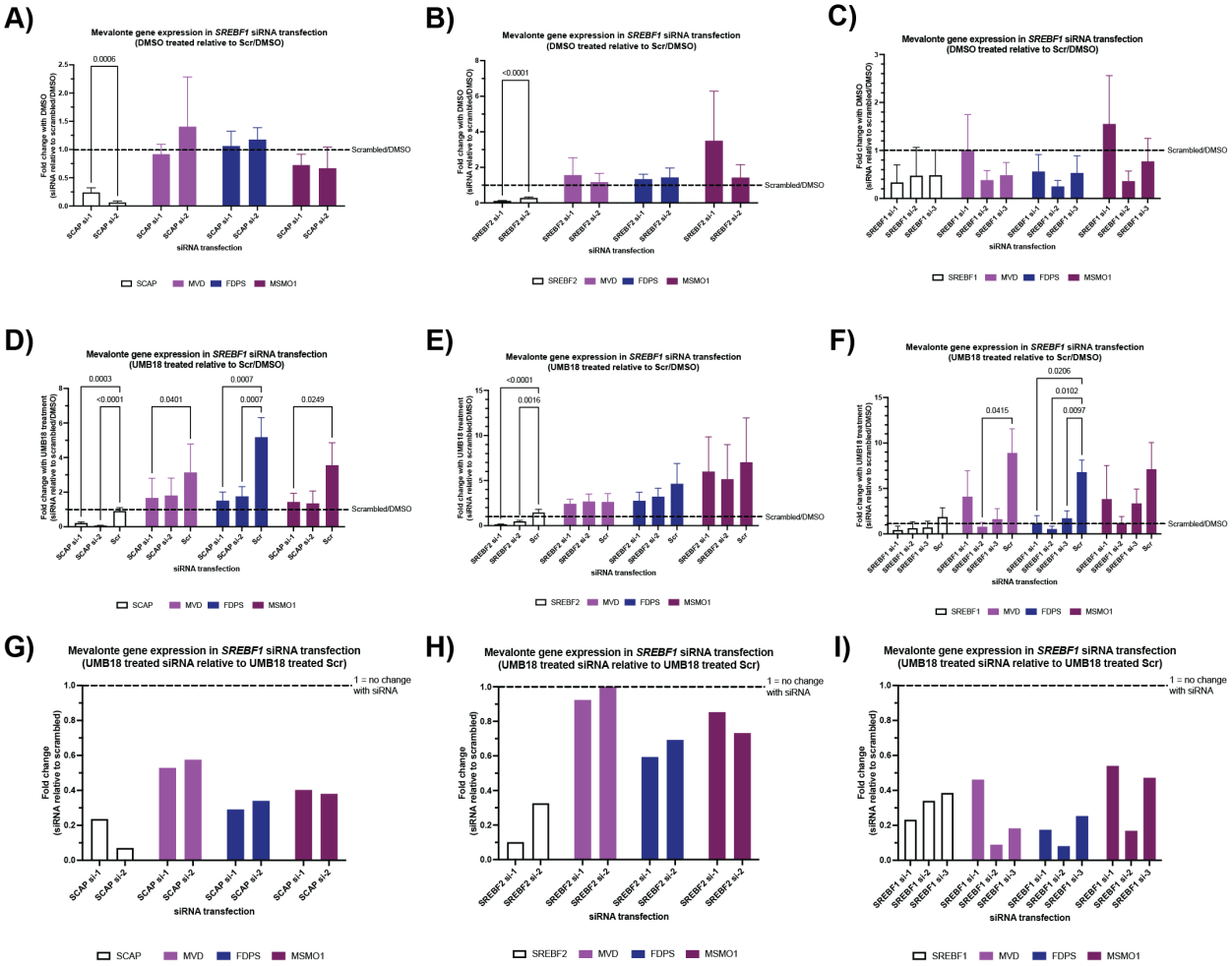

Figure 4 – UMB18 requires SCAP and SREBP genes to increase mevalonate pathway gene expression.

A549-ACE2 cells were transfected with unique siRNA sequences targeting *SCAP* (A, D, G), *Srebf2* (B, E and H) or *Srebf 1* (C, F and I). The cells were then treated with 10μM UMB18 or 0.1% DMSO for 24 h and collected for qRT-PCR targeting the specified genes with normalization to GAPDH as a housekeeping gene. Fold change in gene expression was calculated compared to scrambled siRNA (siScr) transfected cells treated with DMSO (siScr/DMSO) for each of the conditions. A-C) Fold change relative to siScr/DMSO for each of the siRNA transfection conditions with DMSO treatment. Two-way ANOVA analysis was performed for comparison of all conditions and

945 significant p values (<0.05) have been plotted. For all other comparisons within each
946 gene target there were no significant differences between the siRNA sequences. D-F)
947 Fold change relative to siScr/DMSO for UMB18 treatment siRNA transfected cells. Two-
948 way ANOVA analysis were performed for all conditions and significant p-values (<0.05)
949 within each gene target are plotted. Where no p-value has been plotted there were no
950 significant differences within each gene comparison. G-F) As described in Figure 3G,
951 the fold change of UMB18 treated siRNA samples was set relative to the fold change of
952 UMB18 treated siScr and plotted, such that a fold change of 1 would mean no
953 difference between *SCAP/Srebf2/Srebf1* siRNA and scrambled siRNA with UMB18 and
954 a fold change below 1 means a lower change from UMB18 treatment in the targeted
955 siRNA samples. Data are from three independent experiments performed in triplicate in
956 all cases.
957

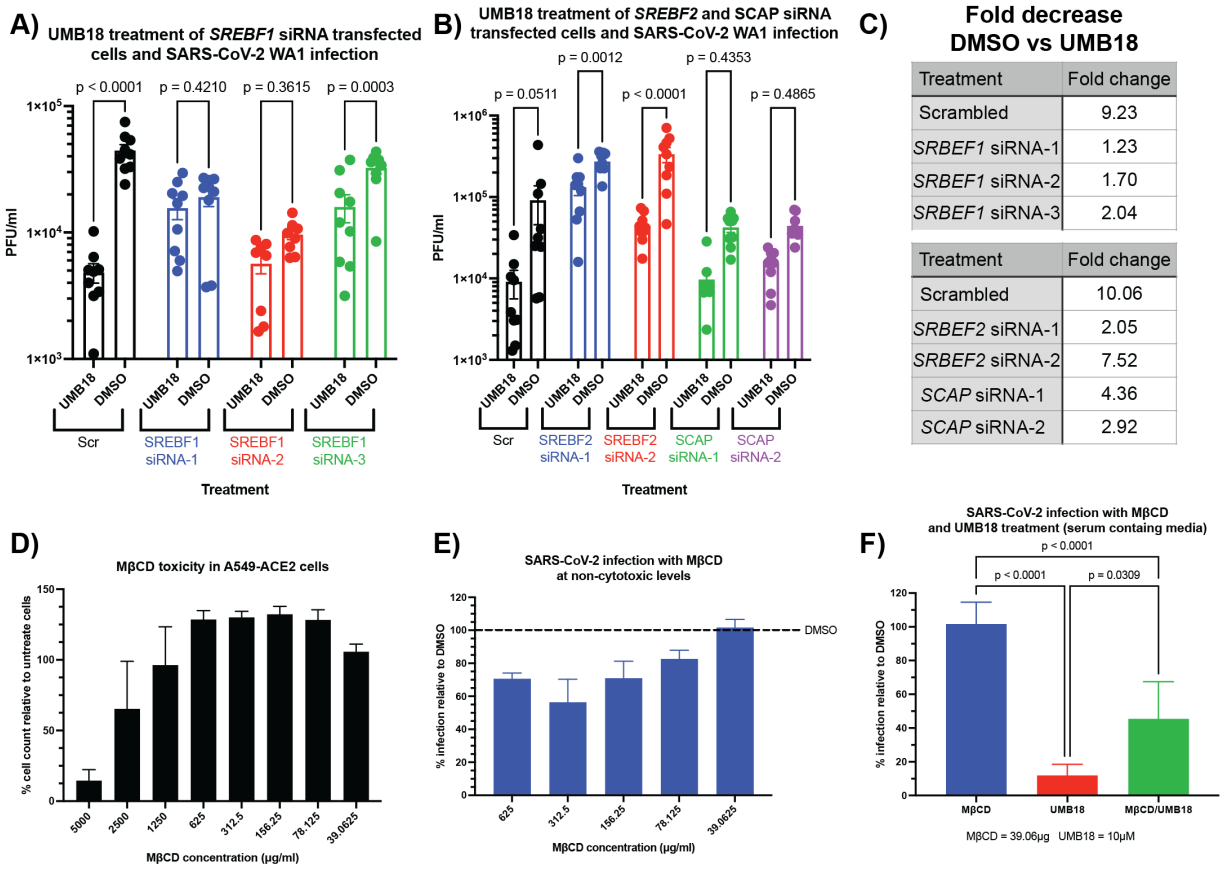

Treatment	Fold change
Scrambled	9.23
SRBEF1 siRNA-1	1.23
SRBEF1 siRNA-2	1.70
SRBEF1 siRNA-3	2.04

Treatment	Fold change
Scrambled	10.06
SRBEF2 siRNA-1	2.05
SRBEF2 siRNA-2	7.52
SCAP siRNA-1	4.36
SCAP siRNA-2	2.92

Figure 5 – Increased cellular cholesterol is required for UMB18-mediated antiviral activity.

A549-ACE2 cells were transfected with siRNA sequences targeting *Srebf1* (A), *SCAP* or *Srebf2* (sequences as used in Figure 4, *SCAP* and *Srebf2* transfections were experimentally performed together while *Srebf1* were performed separately). Following transfection, cells were infected with SARS-CoV-2 at MOI 0.1 and treated with 10µM UMB18 or 0.1% DMSO for 24 h. Supernatant was collected from the cells and viral titer determined by plaque assay on VeroE6 cells expressing TMPRSS2. The titer is plotted as plaque forming units/ml from each of the different transfection and treatment conditions. Using scrambled siRNA (Scr) as the control. Two-way ANOVA analysis was performed and the p-values are plotted. Data are from three independent experiemnts

970 performed in triplicate. C) Fold change between titer of DMSO treated and UMB18
971 treated in each transfection condition summarized in a table format. D) A549-ACE2 cells
972 were treated with the indicated concentrations of methyl-beta-cyclodextrin (MβCD) for
973 24 h prior to fixation with neutral buffered formalin. Cells were stained with Hoechest to
974 label nuclei and cell count per well (96 well format) was quantified with a Celigo high
975 content imager. Reported is the percentage total cell count compared to untreated cells
976 as a measure of cytotoxicity from MβCD treatment. E) A549-ACE2 cells were infected
977 with SARS-CoV-2 at MOI 3 and treated with the indicated concentrations of MβCD for
978 24 h. Cells were similarly fixed with neutral buffered formalin then immunofluorescence
979 labeled for SARS-CoV-2 N protein and stained with Hoechest. High content imaging
980 was used to quantify percentage infection and the plotted data are relative parentage
981 infection compared to untreated control cells. F) As in E, cells were infected with SARS-
982 CoV-2 at MOI 3 and treated with or without MβCD with either 10μM UMB18 or 0.1%
983 DMSO. Cells were similarly fixed and labeled for high content imaging of percentage
984 infection. Plotted are the relative infection percentage to 0.1% DMSO treated cells for
985 each of the different conditions. An unpaired t-test was performed for for each condition
986 and the p-valus are reported. Data are from three independent experiments.
987

988 # Supplemental Figure Captions

989 **Supplemental Figure 1 – Serum impacts UMB18 induced transcriptional changes**
990 **and virus replication.**
991 A and B) A549-ACE2 cells were treated with 10 μM UMB18 or 0.1% DMSO for 24 hours
992 in cell culture media supplemented with serum or without supplementation. Cells were

993 harvested in TRIzol and qRT-PCR performed for the indicated genes. A) Fold change in
994 gene transcript in UMB18 treated cells relative to DMSO treated. B) The same set of
995 experimental data with fold change being in serum free media relative to serum
996 containing media. C) A549-ACE2 cells were infected with SARS-CoV-2 at MOI 0.5 in
997 serum containing or serum free media with 10 μM UMB18 or 0.1% DMSO, or neither
998 and left in just media. 24-hour post infection supernatant was collected and used to titer
999 virus by plaque assay on VeroTMPRSS2 cells. Significance calculated by two-way
1000 ANOVA with a Tukey correction. Only statically significant ($p < 0.05$) comparisons are
1001 shown on the graph.

1002

1003 **Supplemental Figure 2 – UMB18 does not appear to activate mTOR signaling as**
1004 **assessed by phospho-S6K1.**
1005 A) A549-ACE2 cells were plated to plastic and the following day were treated with
1006 100ng recombinant EGF, or PBS carrier alone. At time points between 5 and 30 min,
1007 cells were collected in Triton-X100 lysis buffer and prepared for western blotting (see
1008 Materials and Methods). Samples were separated on gels and blotted for phospho-
1009 S6K1 or S6K1 and tubulin was used as a loading control. All probes were detected with
1010 HRP. Density of bands was determined and quantified by setting relative to tubulin
1011 control and then reported as a relative band density of EGF treated compared to PBS
1012 treated at each time point. B and C) A549-ACE2 cell were plated to plastic and the
1013 following day treated with 10μM UMB18 or 0.1% DMSO for the indicated time points or
1014 left untreated (for 4 hours in B). At each timepoint, cells were collected, and western
1015 blots run similarly to A. All gels were imaged with HRP, except tubulin in B which was

1016 visualized by AlexaFluor 488. Density of UMB18 compared to DMSO at each time point

1017 is reported as in A.

1018

1019